Multimedia Tools and Applications
https://doi.org/10.1007/s11042-022-13192-5

Image denoising using RANSAC and compressive sensing

Isidora Stanković[1] · Miloš Brajović[1] · Jonatan Lerga[2] · Miloš Daković[1] · Ljubiša Stanković[1]

Received: 21 July 2021 / Revised: 21 January 2022 / Accepted: 1 May 2022

Abstract

Image denoising is a vital image processing phase aiming to improve the quality of images and to make them more informative. In this paper, we propose a blind denoising approach for removing the outliers (impulsive disturbances) from digital images, by combining the random sample consensus (RANSAC) and compressive sensing (CS) principles. The proposed approach exploits the fact that images are highly concentrated in the domain of two-dimensional discrete cosine transform (2D-DCT). The sparsity (high concentration) in the transform domain is used in both detection and reconstruction of pixels affected by high disturbances. The image pixels not affected by the noise are found using the RANSAC-based methodology and they are further used as available measurements in the CS reconstruction. The affected pixels are considered unavailable and they are recovered by the CS procedure. The presented approach does not require any disturbance-related assumptions regarding the statistical behavior of the noise or about the range of its values. The theory is verified on examples with 55 images. The comparative analysis against several state-of-the-art methods, done with full-reference and no-reference quality metrics, suggests that the proposed method can be used as an efficient tool for image denoising.

✉ Isidora Stanković
isidoras@ucg.ac.me

Miloš Brajović
milosb@ucg.ac.me

Jonatan Lerga
jlerga@riteh.hr

Miloš Daković
milos@ucg.ac.me

Ljubiša Stanković
ljubisa@ucg.ac.me

[1] Faculty of Electrical Engineering, University of Montenegro, 81000 Podgorica, Montenegro

[2] Faculty of Engineering and Center for Artificial Intelligence and Cybersecurity, University of Rijeka, 51000 Rijeka, Croatia

Published online: 02 June 2022

Keywords Image · Denoising · Impulsive noise · Compressive sensing · Pixel selection · RANSAC

1 Introduction

Within the emerging area of compressive sensing (CS), it is well established that sparse signals can be reconstructed from a reduced number of measurements [3, 5, 6, 9–11, 17, 18, 22, 23, 25, 27, 37, 39, 48, 50, 51, 54]. The CS reconstruction is supported by a rigorous mathematical framework which characterizes the reconstruction process and the quality of the obtained solution, as well as the performance of the reconstruction approaches; it predicts the reconstruction outcome and demystifies the effects caused by unavailable samples (pixels). Digital images can be represented by a small number of nonzero coefficients (or coefficients with significant values, when compared with the remaining coefficients) in the two-dimensional discrete cosine transform (2D-DCT) domain. Therefore, digital images can be considered as sparse (or approximately sparse [8, 42]) in this domain.

The number of samples (pixels) required to reconstruct the signal (image) is related to the number of nonzero coefficients in the sparse domain [9, 22]. Missing observations could arise as a consequence of physical unavailability, restrictions posed by physical phenomena and sensing devices, or could be a part of the sampling strategy (which aims at minimizing the resources - time, energy, memory, required for the data acquisition, transmission and storage, or to minimize the exposure of subjects to a possibly dangerous radiation or chemicals related to the acquisition process). If some signal samples or image pixels are a subject of a high level degradation caused by a strong disturbance, they can be intentionally omitted, considered as unavailable, and recovered using the CS procedures, under the same conditions as otherwise unavailable samples.

Noise represents unwanted content in an image, caused by different sources, such as low light, slow shutter, sensor issues, etc. Sudden, sharp disturbance, known as impulsive noise, is particularly challenging to deal with [40]. This type of noise commonly appears in form of scattered black and white pixels. Primarily, various filters, most commonly median filters, are used as main denoising tools for impulsive disturbance. It is, however, well known that filters only produce approximations, whereas ambiguities in noise characteristics (distribution, unknown positions of affected pixels etc.) cause errors in resulting images [40]. Moreover, affected pixels can appear either in a regular or irregular shape, where regular shapes can be generated due to the defect in the sensor while the irregular shape could possibly be a true feature of the image. These issues serve as a main motivation to develop advanced, non-filtering denoising techniques, based on sophisticated detection and reconstruction of affected pixels. One class of such techniques is based on recent CS paradigm [7, 45, 49].

1.1 Related research

Various methods have been developed in the reconstruction of images affected with random noise, which employ sparsity as the main property driving the denoising process. One of the algorithms based on the sparsity is the Weighted Encoding with Sparse Nonlocal Regularization (WESNR) method from [29]. The algorithm is based on soft impulse pixel detection via weighted encoding used to deal with the noise, while the sparsity prior and non-local self-similarity prior are integrated into a regularization term and introduced into the variational encoding framework.

Two combinations of approaches with the well-known block-matching 3D (BM3D) algorithm [16, 30] are considered as advanced image denoising techniques. The BM3D method is divided into two main steps. After the grouping of similar blocks is performed, a collaborative filtering by shrinkage in the transform domain is done. The blocks are then combined back into a two-dimensional signal. This approach has been combined with the adaptive Kuwahara filter from [4] and a two-stage adaptive filter from [38], which are used for processing of the strong impulsive noise pixels. The adaptive Kuwahara filter [4] is a modification of the Kuwahara filter developed to reduce artefacts in images. The two-stage adaptive method [38] is based on an efficient average filtering algorithm to remove those noisy pixels from the image. The combinations are published in [19, 44].

Another well-known method for denoising images is the total-variation (TV) L1 methodology [12, 35]. The denoising is based on solving a representative minimization problem, assuming that that the image has a high total variation. The main advantage of the TV approach is the preserving details of the images such as the edges. Many forms of the TV denoising approach are the result of a of a research spread over several years [15, 26, 56].

Besides the four algorithms used for comparison in this paper, there are also other techniques developed for the problem at hand. One group of algorithms is based on the hyperspectral denoising [1, 2, 57], such as using the spatio-spectral total variation [1] or using the sparse hyperspetral image representation based on its low-rank and self-similarity characteristics [57]. Denoising algorithms based on deep learning and convolutional neural networks are more frequently engaged recently [31, 55]. Other approaches are based on the variants of the traditional mean and median filters [34, 40], and various other ideas [13, 14, 32, 33, 45].

1.2 The proposed method – relations with previous work and main contributions

In our previous work, we have shown that the CS reconstruction can be characterized by an explicit reconstruction error energy, relating the image sparsity, number of available pixels and total image size [8, 42]. The idea to engage the CS principles and image sparsity in image denoising has been previously presented in [7, 45]. In this paper, we present a more advanced noise detection procedure, based on the random sampling consensus (RANSAC), a widely exploited tool in computer vision, image processing, and other frameworks requiring robust estimation in the presence of a large number of outliers. Pixels disturbed by the impulsive noise can be considered as *outliers* [20, 21, 43]. Other pixels, potentially disturbed by a weak additive noise, are known as *inliers*, and are selected by RANSAC as a consensus set. Furthermore, the subset of pixels chosen by the RANSAC acts as the set of available measurements and is exploited as a basis for the CS reconstruction.

Denoising techniques which combine the CS principles and robust estimation, rely on the fact that the disturbance positions (indices of pixels affected by the disturbance) are known. Unlike such techniques, the proposed methodology operates blindly, without any assumptions regarding the positions of affected pixels, distribution or other characteristics of the noise. We only assume that the image blocks are highly concentrated (i.e. sparse) in the 2D-DCT domain. This assumption is proved to be valid in the CS-based image recovery [8, 42].

The proposed technique is characterized by its ability to detect the pixels affected by the disturbance even in the challenging case when the corruption is within the pixel value range. This is achieved through RANSAC-based selection of suitable pixels, driven by sparsity (concentration) measures and inspired by the compressive sensing framework. These suitable pixels are inliers. In general, they can be affected only by a low noise. The other, highly corrupted pixels represent outliers. A disturbance in a pixel will affect all corresponding 2D-DCT coefficients, by degrading the transform sparsity (concentration). Detection of such event is carefully integrated within the RANSAC adaptation presented in this paper. Starting from a random set of measurements, for each image block, a set of successive CS reconstructions is performed until an outlier-free consensus set with a sufficient number of elements is found. This means that for the observed image block, a set of inliers is selected, and further used in a CS procedure as a set of available measurements. The other, thrown away pixels (labeled by RANSAC approach as outliers and therefore as unavailable) are recovered by the CS algorithm. The proposed approach can provide an exact reconstruction if the selected inliers are noise-free, rather than producing a filtered approximation of the original image. The method presented in this paper is an extension of the one-dimensional approach recently proposed in [43] to the image processing and the 2D-DCT.

The paper is organized as follows. After short Introduction, in Section 2 we present basic theoretical background regarding the sparse image representation in the 2D-DCT domain, including the basic CS principles. In Section 3, the proposed RANSAC-based denoising procedure is presented, which exploits the CS reconstruction on pixels affected by the disturbance. The theory is validated on numerical examples in Section 4. Concluding remarks are given at the end of the paper.

2 Basic definitions

2.1 Sparse image representation

Two-dimensional discrete cosine transform (2D-DCT) is typically exploited in various digital image processing algorithms. For an image $x(n,m)$ of size $N \times M$, the 2D-DCT is defined as

$$X(k,l) = \mathscr{T}\{x(n,m)\} = \sum_{n=0}^{N-1}\sum_{m=0}^{M-1} x(n,m)\varphi(n,m,k,l), \tag{1}$$

with basis functions, $\varphi(n,m,k,l)$, of the form

$$\varphi(n,m,k,l) = c_k c_l \cos\left(\frac{\pi(2N+1)k}{2N}\right)\cos\left(\frac{\pi(2M+1)l}{2M}\right), \tag{2}$$

where constants c_k and c_l are given by

$$c_k = \begin{cases} 1/\sqrt{N}, & \text{for } k=0 \\ \sqrt{2/N}, & \text{for } k \neq 0 \end{cases} \quad c_l = \begin{cases} 1/\sqrt{M}, & \text{for } l=0 \\ \sqrt{2/M}, & \text{for } l \neq 0. \end{cases} \tag{3}$$

Strong involvement in digital image processing and related applications 2D-DCT mainly owes to its ability to represent entire images (or blocks within those images) with a small number of nonzero coefficients or coefficients with significant values, with the remaining coefficients being zero-valued, or at least being close to zero.

The original image, $x(n,m)$, is obtained from its 2D-DCT coefficients, $X(k,l)$, based on the inverse 2D-DCT defined as follows

$$x(n,m) = \mathscr{T}^{-1}\{X(k,l)\} = \sum_{k=0}^{N-1}\sum_{l=0}^{M-1} X(k,l)\psi(n,m,k,l). \tag{4}$$

This inverse transform has the same basis functions, $\psi(n,m,k,l) = \varphi(n,m,k,l)$, as the corresponding direct transform. Formulations (1) and (4) can be compactly rewritten using matrix equations,

$$\mathbf{X} = \Phi\mathbf{x} \quad \text{and} \quad \mathbf{x} = \Phi\mathbf{X}, \tag{5}$$

where matrix Φ of size $MN \times MN$ is obtained as

$$\Phi = \Phi^{1D}_{N\times N} \otimes \Phi^{1D}_{M\times M}, \tag{6}$$

with $\otimes$ used to denote the Kronecker product of one dimensional DCT matrices $\Phi^{1D}_{N\times N}$ and $\Phi^{1D}_{M\times M}$.

The direct and inverse 2D-DCT are commonly rearranged from the four-dimensional to a two-dimensional space using the stacked vector forms of the image and its DCT transform,

$$\begin{aligned} x(n,m) &= x_v(n + N(m-1)) = x_v(p) \\ X(k,l) &= X_v(k + N(l-1)) = X_v(q), \end{aligned} \tag{7}$$

which results in the transformation matrix elements of the form

$$a(p,q) = a(n + N(m-1), k + N(l-1)) = \varphi(n,m,k,l), \tag{8}$$

where $p = n + N(m-1)$ and $q = k + N(l-1)$.

Notice that instead of considering the whole $N \times M$ image, the image is commonly divided into non-overlapping blocks, $x_b(n,m)$, of size $B \times B$. Then all the previous relations hold for individual blocks $x_b(n,m)$ with summation limits from 0 to $B-1$.

An image block $x_b(n,m)$ can be represented with only K of nonzero 2D-DCT transformation elements, $K \ll B^2$. This K-sparse block can be expressed as

$$x_b(n,m) = \sum_{i=1}^{K} X_b(k_i,l_i)\varphi(n,m,k_i,l_i) = \sum_{i=1}^{K} A_i\varphi(n,m,k_i,l_i), \tag{9}$$

with $i = 1, 2, \ldots, K$, where A_i are nonzero transform coefficients $X_b(k,l)$ at $(k,l) = (k_i,l_i) \in \mathbb{K} = \{(k_1,l_1), (k_2,l_2) \ldots (k_K,l_K)\}$. In other words, the whole information from the b-th block is contained within only K nonzero 2D-DCT coefficients.

2.2 Compressive sensing reconstruction of sparse images

In the light of the compressive sensing theory, sparse image blocks, $x_b(n,m)$, can be reconstructed from a reduced set of pixels at positions $(n_j,m_j) \in \mathbb{N}_A$, $j = 1, 2, \ldots, N_A$, where

$$\mathbb{N}_A \subseteq \mathbb{N} = \{(n,m) \mid 0 \le n \le N-1,\ 0 \le m \le M-1\}. \tag{10}$$

The reduced set of pixels can be considered as a set of N_A measurements. Each measurement is a linear combination of nonzero 2D-DCT coefficients, that is

$$x_b(n_j,m_j) = \sum_{k=0}^{B-1}\sum_{l=0}^{B-1} X_b(k,l)\varphi(k,l,n_i,m_i). \tag{11}$$

This can be further rewritten more compactly, in a stacked vector form, by taking into account notation in (7), as

$$x_b(n_j,m_j) = y_b(j) = \sum_{q=0}^{B^2-1} X_{vb}(q)a(p_j,q), \tag{12}$$

with $j = 1, 2, \ldots, N_A$, or in terms of matrix equations, as

$$\mathbf{y}_b = \mathbf{A}\mathbf{X}_b, \tag{13}$$

with measurement vector, $\mathbf{y}_b$, of size $N_A \times 1$,

$$\mathbf{y}_b = [y_b(1), y_b(2), \ldots, y_b(N_A)]^T \tag{14}$$
$$= [x_b(n_1, m_1), x_b(n_2, m_2), \ldots, x_b(n_{N_A}, m_{N_A})]^T. \tag{15}$$

The measurement matrix, $\mathbf{A}$, in (13) consists of elements $a(p_j, q)$, with indices p_j corresponding to the available pixels, $p_j = n_j + N(m_j - 1)$, $j = 1, 2, \ldots, N_A$, and $q = k + N(l - 1)$, as given by (7) and (8). The 2D-DCT coefficient vector, $\mathbf{X}_b$, corresponding to the stacked vector form in (7) is given by

$$\mathbf{X}_b = [X_{vb}(0), X_{vb}(1), \ldots, X_{vb}(B^2 - 1)]^T. \tag{16}$$

Compressive sensing reconstruction can be performed on each $B \times B$ image block separately. CS reconstruction procedures aim to determine the unknown coefficient vector, $\mathbf{X}_b$ which satisfies the under-determined system of measurement equations, $\mathbf{y}_b = \mathbf{A}\mathbf{X}_b$, and is, at the same time, the sparsest possible solution (among infinitely many possible solutions) of this system. More formally, this problem can be formulated as a minimization of the following form [3, 9, 22]

$$\min \|\mathbf{X}_b\|_0 \text{ subject to } \mathbf{y}_b = \mathbf{A}\mathbf{X}_b, \tag{17}$$

where $\|\mathbf{X}_b\|_0$ denotes the ℓ_0 (pseudo)-norm of the vector $\mathbf{X}_b$, being in fact the number of nonzero elements in $\mathbf{X}_b$ (cardinality). A reconstruction method which solves (17) and belongs to the orthogonal matching pursuit (OMP) class of the algorithms will be presented as an integral part of the proposed denoising procedure.

Previous problem formulation is crucial for the considered denoising framework. As it will be shown next, if we are able to (blindly) detect the unknown positions of disturbed image pixels, then these pixels can be simply eliminated and considered as unavailable, whereas the compressive sensing reconstruction procedures could be engaged to provide adequate replacements, with the remaining pixels considered as available measurements. This is discussed in detail in Section 3.2.

3 Reconstruction of sparse images with outliers

Although the original CS formulation in image processing deals with the reconstruction of the image from a reduced set of available pixels, the compressive sensing approach can be used in image denoising problems, when all pixels are available. Specifically, in the scenario when some of the image pixels are heavily affected by a high noise, these pixels can be declared as unavailable and reconstructed based on the remaining pixels acting as the compressive sensing measurements [49].

The strategy of engaging the CS in image denoising consists of two crucial steps: (i) detection of pixels affected by the noise, which are thrown away from further analysis (considered as unavailable) and (ii) reconstruction of these unavailable pixels using only the set of remaining pixels (not affected by the noise). Therefore, it is crucial to develop a methodology which can automatically and blindly determine positions of pixels affected by the noise. In early papers on compressive sensing denoising, the salt and pepper noise was assumed when the noisy pixels were detected by simple thresholding. Extremely high and low pixels intensities were declared as noisy and removed before the reconstruction [45, 49]. However, these approaches were not able to deal with noise in the pixels within the range of other pixel intensities. For detection of such pixels a sparsity measure approach was proposed [45]. This method, in combination with the sparsity measure gradient estimation and image blocks overlapping, produced good detection results, followed by accurate recovery of disturbed pixels. However, a quite high calculation burden is the main drawback of this approach.

In this Section, we will present a RANSAC-based approach for the selection of the pixels for the image reconstruction. It provides a blind detection of disturbed pixels, which are removed and recovered by engaging a compressed sensing reconstruction procedure. This method will produce an efficient recovery of disturbed pixels, and is characterized by a reduced calculation complexity.

3.1 Noisy image model

Consider a digital image $x(n, m)$, $0 \leq n \leq N-1$, $0 \leq m \leq M-1$. The image can be divided into $B \times B$-sized non-overlapping blocks of pixels. Without loss of generality, we may assume that $N = N_B B$ and $M = M_B B$, where N_B and M_B are integers. As it is commonly done [24, 46], it is reasonable to assume that the set of 2D-DCT coefficients of considered $B \times B$-sized pixel blocks is sparse, for each considered block.

Next, assume that the image is corrupted by two kinds of noise:

- A small noise $\varepsilon(n, m)$. The pixels with this kind of noise can be considered acceptable for signal reconstruction (inliers). This kind of noise will result in a small reconstruction error in the resulting image.
- An impulsive, high, noise $\nu(n, m)$ in some of the image pixels. The number of pixels with impulsive noise in the block is denoted by I and this number is significantly lower than B^2. These disturbances are located at unknown positions $(n, m) \in \mathbb{N}_I \subseteq \mathbb{N}$.

  Commonly, impulsive noise, $\nu(n, m)$, is modelled assuming that

  - $\nu(n, m) = 0$ for $(n, m) \notin \mathbb{N}_I$;
  - $\nu(n, m)$ takes arbitrary high values for $n \in \mathbb{N}_I$.

  These pixels are outliers and should be removed before the image is reconstructed using the compressive sensing methods.

The original image can be fully recovered if a sufficient number of inlier pixels exists. The sufficient number of inliers is directly related to the full recovery conditions studied in the CS theory [9, 22, 37]. A rough estimation of the smallest number of samples that should be used in the reconstruction of K sparse signal can be made based on the statistical results presented in [9].

The selection of appropriate samples for the compressive sensing reconstruction will be based on the RANSAC.

3.2 RANSAC in image denoising

The considered noisy image model is given by

$$x(n, m) = s(n, n) + \varepsilon(n, m) + \nu(n, m) \tag{18}$$

where $s(n, m)$ is the original noise-free image, with pixel blocks of size $B \times B$ being sparse in the 2D-DCT domain, $\varepsilon(n, m)$ is a Gaussian noise with a small variance σ_ε (inliers), while $\nu(n, m)$ is a high impulsive noise (outliers). Next, we present a procedure for blind detection of outliers, outlined in Algorithm 1.

1. The considered image block $x_b(n,m)$ is K-sparse. Select a small subset $\mathbb{S}$ with S randomly positioned pixels $x(n,m)$ at $(n,m) \in \mathbb{S}$, such that the reconstruction for a K-sparse image block is possible.
2. The pixels from $\mathbb{S}$ are used to reconstruct the whole image block, $x_{Rb}(n,m)$, at all pixel positions (n,m), $n = 0,1,2,\ldots,B-1$, $m = 0,1,2,\ldots,B-1$. The reconstruction is done based on the compressive sensing principles. Based on the set of measurement equations

$$x_b(n_j,m_j) = y_b(j) = \sum_{i=1}^{K} \hat{X}_{vb}(q_i)a(p_j,q_i), \tag{19}$$

$j = 1,2,\ldots,N_A$, CS reconstruction procedure aims at finding the set of elements $\hat{X}_{vb}(q_i)$ satisfying the given equations, and being the sparsest possible solution at the same time. This corresponds to the minimization in (17). One approach to solve this problem is a two-step strategy, defined as follows:

Step 1: Detect the positions of nonzero elements,
Step 2: Apply an algorithm for reconstruction with known positions of nonzero elements as in the standard RANSAC.

The linear nature of the relation between the randomly selected samples, $x(n_j,m_j)$, for the given 2D-DCT elements, indicates that a back-projection of the measurement vector, $\mathbf{y}_b$, to the measurement matrix, $\mathbf{A}$, can be used as the tool for the nonzero element position estimation, that is

$$\mathbf{X}_{b0} = \mathbf{A}^H\mathbf{y}_b. \tag{20}$$

In an ideal case, the matrix $\mathbf{A}^H\mathbf{A}$ ensures that the initial estimate, $\mathbf{X}_{b0}$, contains exactly K elements at positions $\{q_1,q_2,\ldots,q_K\}$ for which the magnitudes are larger than the largest magnitudes at the remaining positions. By taking the positions of these largest magnitude elements in $\mathbf{X}_{b0}$ as the set $\{q_1,q_2,\ldots,q_K\}$, the signal can be reconstructed based on the pseudo-inversion

$$\mathbf{X}_{bK} = (\mathbf{A}_K^H\mathbf{A}_K)^{-1}\mathbf{A}_K^H\mathbf{y}_b = \mathrm{pinv}(\mathbf{A}_K)\mathbf{y}_b, \tag{21}$$

with $\mathbf{A}_K$ obtained from the measurement matrix $\mathbf{A}$, by keeping columns with indices $\{q_1,q_2,\ldots,q_K\}$. The reconstructed image in the block b is then

$$x_b(n,m) = \sum_{i=1}^{K} \hat{X}_b(k_i,l_i)\varphi(n,m,k_i,l_i) \tag{22}$$

where $\hat{X}(k,l)$ are zero-valued at all (k,l), $0 \le k \le B-1$, $0 \le l \le B-1$, except for

$$(k,l) \in \{(k_1,l_1),(k_2,l_2),\ldots,(k_K,l_K)\},$$

where $\hat{X}_b(k_i,l_i) = X_{bK}(q_i)$.

The procedure can be iteratively implemented, in the form of Matching Pursuit [47]. The implementation is presented in the Algorithm 2.
3. After the image block is reconstructed, for every pixel $x_b(n,m)$, $n,m = 0,1,\ldots,B-1$, the corresponding distance d_{nm}, from the estimated signal $x_{Rb}(n,m)$ is calculated,

$$d_{nm} = |x_{Rb}(n,m) - x_b(n,m)|. \tag{23}$$

4. If a sufficient number of pixels is such that their distance from the reconstructed model is lower than the assumed threshold, for example, $d = 2.5\sigma_\varepsilon$, then all these pixels are

included in a new set of available pixels

$$\mathbb{D} = \{x_b(n,m)| \quad d_{n,m} \leq d\}, \tag{24}$$

and the final reconstruction of the image block is calculated with all data from $\mathbb{D}$. Note that the robust estimation of the standard deviation can be done using median absolute deviation (MAD), defined by

$$MAD_x = \underset{n,m=0,1,\dots,B-1}{\text{median}} \left\{ \left| x_b(n,m) - \underset{n,m=0,1,\dots,B-1}{\text{median}} \{x_b(n,m)\} \right| \right\}. \tag{25}$$

The MAD value is related to the sample standard deviation as $MAD_x = 0.6745\sigma_x$ (for the Gaussian random variable).

5. If there is no sufficient number of pixel values within the distance d, that is, card$\{\mathbb{D}\} < T = B^2/2$, a new random small set of pixels, $i \in \mathbb{S}$, is taken and the procedure is repeated from point 2.
6. The procedure is stopped when the desired number of data points within $\mathbb{D}$ is achieved, card$\{\mathbb{D}\} \geq T = B^2/2$ or the maximum number of trials N_{max} is reached.

The previously described denoising approach is summarized in Algorithm 1, which will be used and compared in the numerical examples presented in this paper. It exploits a matching pursuit CS reconstruction procedure, CSREC·, summarized in Algorithm 2. The flowchart of approach is presented in Fig. 1 for a single image block denoising.

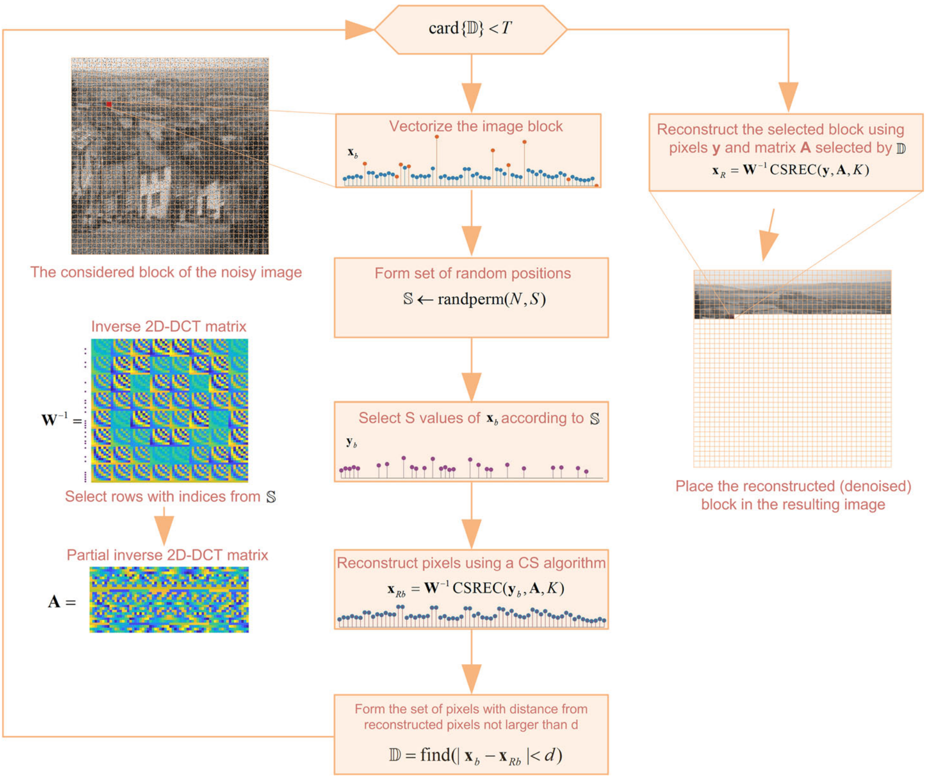

Fig. 1 The flowchart of the RANSAC-based denoising algorithm, presented for a single $B \times B$ image block

The presented RANSAC-based denoising algorithm will produce the same results if other CS reconstruction methodologies are used instead of the OMP, such as, for instance, the Bayesian CS reconstruction or the iterative hard thresholding (IHT). An overview of these procedures can be found in [41, 47].

Algorithm 1 RANSAC CS denoising algorithm.

Input: Noisy image block $\mathbf{x}_b$, RANSAC set size S, bound for inliers d, threshold for the consensus number of pixels T, maximum number of iterations N_{max}, image block sparsity K

$D \leftarrow 0$, $N_{it} \leftarrow 0$
while $D < T$ and $N_{it} \leq N_{max}$ **do**
  $N_{it} \leftarrow N_{it} + 1$
  $\mathbb{S} \leftarrow \text{randperm}(N, S)$, ▷ S random numbers from the first N natural numbers
  $\mathbf{A} \leftarrow$ rows of the inv. 2D-DCT matrix selected by the set $\mathbb{S}$
  $\mathbf{y}_b \leftarrow$ elements of $\mathbf{x}_b$ selected by the set $\mathbb{S}$
  $\mathbf{X}_b \leftarrow \text{CSREC}(\mathbf{y}_b, \mathbf{A}, K)$ ▷ Algorithm 2
  $\mathbf{x}_{Rb} = \mathbf{W}^{-1}\mathbf{X}_b$
  $\mathbb{D} = \text{find}(|\mathbf{x}_b - \mathbf{x}_{Rb}| < d)$,
  $D = \text{card}(\mathbb{D})$, ▷ the number of elements in $\mathbb{D}$
end while

Perform the CS reconstruction with the consensus set $\mathbb{D}$:

$\mathbf{A} \leftarrow$ rows of the inverse DFT matrix $\mathbf{W}^{-1}$ selected by set $\mathbb{D}$
$\mathbf{y} \leftarrow$ elements of $\mathbf{x}$ selected by the set $\mathbb{D}$
$\mathbf{X} \leftarrow \text{CSREC}(\mathbf{y}, \mathbf{A}, K)$
$\mathbf{x}_R \leftarrow \mathbf{W}^{-1}\mathbf{X}$

Output: Reconstructed denoised image block $\mathbf{x}_R$

Algorithm 2 Matching pursuit CS reconstruction.

function $\text{CSREC}(\mathbf{y}_b, \mathbf{A}, K)$
  $\mathbb{K} \leftarrow \emptyset$, $\mathbf{e} \leftarrow \mathbf{y}_b$,
  for $i = 1$ to K **do**
    $k \leftarrow$ position of the largest value in $|\mathbf{A}^H\mathbf{e}|$
    $\mathbb{K} \leftarrow \mathbb{K} \cup k$
    $\mathbf{A}_K \leftarrow$ columns of the measurement matrix $\mathbf{A}$ selected by the set $\mathbb{K}$
    $\mathbf{X}_{Kb} \leftarrow \text{pinv}(\mathbf{A}_K)\mathbf{y}_b$
    $\mathbf{y}_{Kb} \leftarrow \mathbf{A}_K\mathbf{X}_{Kb}$
    $\mathbf{e} \leftarrow \mathbf{y}_b - \mathbf{y}_{Kb}$
  end for
  $\mathbf{X}_b \leftarrow \mathbf{0}$, $\mathbf{X}_b \leftarrow \mathbf{X}_{Kb}$ for $k \in \mathbb{K}$
  return $\mathbf{X}_b$
end function

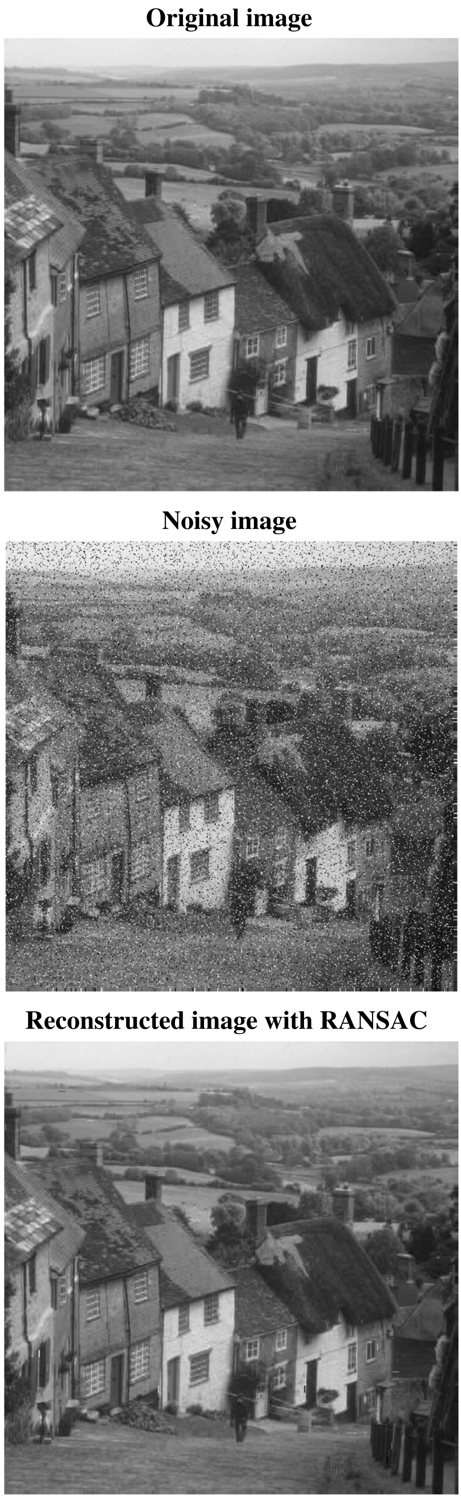

Fig. 2 Denoising of image "Goldhill" with 15% of outliers: original image (top), noisy image (middle), reconstructed using a combination of RANSAC and OMP (bottom)

Fig. 3 The dataset of 55 test images used in the comparative analysis in Example 2

4 Results

Example 1: Reconstruction results The reconstruction will be performed using the image "Goldhill" of size $N \times M = 512 \times 512$. The image is presented in Fig. 2 (top). The image assumes that 15% of the pixels are affected by impulsive disturbance, which means that in average $I = 9.6$ pixels per block are highly affected (but not necessarily salt and pepper noise). This case is illustrated in Fig. 2 (middle).

The RANSAC-based detection algorithm starts from the subset $\mathbb{S}$ of 40% randomly selected pixels, which can be either affected or not affected by the disturbance. These samples are used as the CS measurements. Upon performing the reconstruction, the RANSAC determines how much does the obtained solution, representing the linear model for the measurements, fits the pixels from the observed image block, and determines the consensus set $\mathbb{D}$. If $\text{card}\{\mathbb{D}\} < T = B^2/2$, the procedure is repeated for the next random subset of measurements, until the outlier-free subset is found. The noisy image is shown in Fig. 2 (middle). The final recovery result is shown in Fig. 2 (bottom).

Example 2: Statistics on test image set The proposed algorithm is compared with competitive methods on a set of 55 test images. The considered set of images consists of 49 images from the database found at [28] and additional six standard MATLAB test images. The dataset is 49 images of size 512×512. Additionally, image 50 is of size 291×240, image 51 is 205×345, the image 52 is of size 256×320, the image 53 is of size 384×512, image 54 is of size 486×732 and image 55 is of size 512×512.

The images are shown in Fig. 3. We assume that the images are affected by 10% of random valued impulsive noise. The noisy dataset is shown in Fig. 4. Images are denoised using the proposed algorithm. The resulting set of images is shown in Fig. 5.

The comparison has been performed using two full-reference quality measures, the peak-to-noise ratio (PSNR) and the multi-scale structural similarity index (MS-SSIM). Based on the original image $s(n, m)$ and reconstructed image, $x_R(n, m)$, the PSNR is calculated as

$$PSNR = 10 \log_{10} \left(\frac{255^2}{\frac{1}{NM} \sum_{n=0}^{N-1} \sum_{m=0}^{M-1} |s(n, m) - x_R(n, m)|^2} \right). \tag{26}$$

The MS–SSIM from [53] is a more robust version of the well-known structural similarity (SSIM) index, which is calculated as [52]

$$SSIM = \frac{(2\mu_s \mu_{x_R} + c_1)(2\sigma_{s x_R} + c_2)}{(\mu_s^2 + \mu_{x_R}^2 + c_1)(\sigma_s^2 + \sigma_{x_R}^2 + c_2)}, \tag{27}$$

with μ_s, μ_{x_R}, c_1, σ_s^2, c_1 and c_2 being statistical parameters defined in [52]. The value of the MS–SSIM parameter is between 0 (no similarity) and 1 (full similarity).

Moreover, a no-reference quality measure, the Naturalness Image Quality Evaluator (NIQE), introduced in [36], was used for the evaluation of the performance. For the analysis of this parameter, the smaller value, the more natural the image looks.

We compare the results of the proposed method with four other algorithms: the WESNR algorithm from [29], a combination of an adaptive Kuwahara [4] and BM3D [16, 30], presented in [19], a combination of a two-stage adaptive filter [38] with BM3D, presented in [44], and with the total variation L1 algorithm from [12, 35, 56]. The results are shown in

Fig. 4 The noisy dataset of 55 test images used in the comparative analysis in Example 2

Fig. 5 The reconstructed dataset of 55 test images used in the comparative analysis in Example 2

Table 1 PSNR for the dataset of test images

Test image	Proposed	TV-L1	Kuwahara-BM3D	Zayed-BM3D	WESNR
1	**41.57**	22.81	26.54	23.35	28.27
2	**32.12**	26.11	21.88	23.69	26.66
3	**28.77**	26.96	27.71	24.21	24.45
4	**40.54**	19.22	20.07	17.35	22.13
5	**47.06**	27.49	26.95	22.70	28.71
6	**26.39**	23.53	23.14	21.26	23.34
7	**33.08**	19.51	20.40	18.21	21.24
8	12.96	**26.51**	25.24	25.84	26.03
9	20.22	24.03	18.13	23.54	**25.61**
10	**28.78**	25.44	20.41	23.79	28.04
11	**19.87**	19.41	19.02	17.54	19.18
12	**33.16**	21.57	22.60	17.51	23.56
13	16.45	24.82	23.01	24.14	**28.41**
14	**48.64**	20.02	22.89	20.25	23.06
15	**39.88**	21.22	22.79	19.64	21.51
16	**48.71**	21.78	22.01	21.27	23.81
17	15.55	22.03	19.25	20.45	**25.72**
18	**25.96**	19.67	21.84	19.51	20.69
19	14.26	23.32	23.79	21.90	**25.58**
20	**34.75**	21.96	23.08	21.64	25.67
21	19.67	26.28	27.44	21.54	**29.43**
22	**47.52**	23.21	24.26	23.40	24.48
23	14.34	28.26	27.33	22.28	**31.47**
24	28.88	27.06	27.58	27.62	**30.23**
25	20.26	10.02	**23.79**	11.79	21.27
26	**44.53**	26.69	26.58	27.86	29.16
27	17.98	29.36	17.97	23.80	**25.49**
28	**34.76**	23.46	26.45	26.48	27.63
29	**43.69**	20.07	20.52	16.14	21.60
30	**43.55**	24.87	25.30	23.91	28.13
31	**46.09**	18.98	21.55	15.52	21.46
32	15.30	23.71	15.25	21.05	**24.63**
33	**29.48**	25.91	25.89	23.25	29.02
34	**46.17**	23.74	24.28	24.29	26.98
35	**32.35**	25.21	24.58	25.33	27.99
36	13.70	22.50	25.90	20.02	**26.58**
37	**48.88**	24.34	25.08	25.06	23.40
38	21.66	21.62	23.30	24.23	**25.58**
39	18.69	**26.63**	26.02	23.32	15.97
40	**47.41**	26.53	26.37	29.16	26.22
41	**35.59**	26.51	28.23	25.24	31.59

Table 1 (continued)

Test image	Proposed	TV-L1	Kuwahara-BM3D	Zayed-BM3D	WESNR
42	**52.75**	24.46	25.20	21.73	24.77
43	19.33	**26.15**	17.33	23.96	24.82
44	**41.42**	15.61	18.26	13.48	18.44
45	**30.18**	25.79	24.10	25.64	29.13
46	**27.91**	23.79	23.60	23.02	26.63
47	**35.76**	18.94	23.40	20.27	23.13
48	**32.89**	25.63	26.05	26.73	29.03
49	**17.87**	17.54	8.397	16.86	15.37
50	18.04	28.50	25.74	24.51	**29.73**
51	**38.26**	24.19	21.53	23.34	27.16
52	**49.53**	26.47	26.00	27.76	28.02
53	**46.93**	32.32	29.37	30.64	34.92
54	**45.92**	30.61	24.68	30.80	30.20
55	**43.59**	33.58	29.40	28.84	35.61

The results are obtained by the proposed, two-stage (2-stage) adaptive [38] and BM3D [16], presented in [44], Kuwahara-BM3D from [19], the total variation L1 [12, 35, 56], and WESNR from [29] methods. The noise assumed to be in 10% of the pixels affected by random valued impulsive noise

Bold values indicate the method with the best performance for the respective quality measure

Tables 1, 2, and 3, with three different objective quality measures acting as the comparative criteria.

As it can be seen from the tables, the proposed denoising technique shows better results in most of the images tested. In cases where it showed more favorable results, the proposed

Table 2 MS–SSIM for the dataset of test images

Test image	Proposed	Kuwahara-BM3D	Zayed-BM3D	TV-L1	WESNR
1	**0.99**	0.92	0.95	0.92	0.98
2	**0.97**	0.91	0.90	0.94	0.96
3	**0.98**	0.92	0.92	0.91	0.97
4	**0.99**	0.90	0.91	0.93	0.95
5	**0.99**	0.93	0.93	0.96	0.97
6	**0.97**	0.91	0.90	0.92	0.96
7	**0.99**	0.85	0.91	0.81	0.93
8	**0.92**	0.91	0.87	0.93	0.91
9	0.92	0.92	0.87	0.91	**0.96**
10	**0.98**	0.94	0.83	0.98	0.94
11	**0.94**	0.86	0.87	0.81	0.91
12	**0.98**	0.92	0.89	0.94	0.96
13	0.91	0.92	0.88	0.95	**0.96**
14	**0.99**	0.80	0.90	0.83	0.93
15	**0.99**	0.84	0.89	0.84	0.94
16	**0.99**	0.83	0.84	0.81	0.91
17	0.95	0.90	0.83	0.91	**0.96**

Table 2 (continued)

Test image	Proposed	Kuwahara-BM3D	Zayed-BM3D	TV-L1	WESNR
18	**0.97**	0.83	0.90	0.82	0.91
19	0.93	0.92	0.92	0.92	**0.96**
20	**0.99**	0.86	0.89	0.88	0.95
21	**0.98**	0.90	0.91	0.91	0.95
22	**0.99**	0.89	0.92	0.90	0.94
23	0.94	0.95	0.92	0.95	**0.97**
24	**0.96**	0.93	0.93	0.94	0.96
25	**0.98**	0.87	0.92	0.92	0.96
26	**0.99**	0.91	0.90	0.94	0.96
27	0.89	**0.96**	0.89	0.95	0.96
28	**0.99**	0.93	0.93	0.94	0.96
29	**0.99**	0.86	0.86	0.87	0.94
30	**0.99**	0.88	0.89	0.89	0.94
31	**0.99**	0.86	0.90	0.86	0.93
32	**0.95**	0.91	0.78	0.92	0.95
33	**0.98**	0.90	0.90	0.91	0.96
34	**0.99**	0.90	0.91	0.92	0.96
35	**0.99**	0.94	0.94	0.95	0.97
36	0.93	0.90	0.93	0.91	**0.96**
37	**0.99**	0.83	0.84	0.87	0.93
38	**0.96**	0.92	0.91	0.93	0.96
39	**0.94**	0.93	0.90	0.94	0.93
40	**0.99**	0.91	0.89	0.96	0.96
41	**0.99**	0.93	0.94	0.95	0.98
42	**0.99**	0.92	0.93	0.95	0.96
43	0.92	0.94	0.90	0.95	**0.97**
44	**0.99**	0.77	0.84	0.72	0.89
45	**0.98**	0.93	0.90	0.96	0.96
46	**0.99**	0.89	0.91	0.90	0.96
47	**0.98**	0.84	0.91	0.86	0.95
48	**0.99**	0.94	0.92	0.96	0.97
49	**0.97**	0.87	0.61	0.83	0.81
50	0.97	0.95	0.90	**0.98**	0.97
51	**0.99**	0.92	0.87	0.93	0.95
52	**0.99**	0.91	0.91	0.93	0.95
53	**0.99**	0.97	0.95	0.99	0.98
54	**0.99**	0.94	0.91	0.97	0.96
55	**0.99**	0.97	0.93	0.98	0.98

The results are obtained by the proposed, two-stage (2-stage) adaptive [38] and BM3D [16], presented in [44], Kuwahara-BM3D from [19], the total variation L1 [12, 35, 56], and WESNR from [29] methods. The noise assumed to be in 10% of the pixels affected by random valued impulsive noise

Bold values indicate the method with the best performance for the respective quality measure

Table 3 NIQE for the dataset of test images

Test image	Proposed	Kuwahara-BM3D	Zayed-BM3D	TV-L1	WESNR
1	**6.14**	17.42	14.71	13.73	9.59
2	**7.91**	19.39	16.99	9.21	9.70
3	**6.73**	17.88	15.87	11.15	9.78
4	**7.79**	16.95	15.44	12.50	9.02
5	**8.71**	15.66	17.18	13.65	11.56
6	**7.88**	17.53	12.17	8.74	8.27
7	8.97	18.36	14.01	11.19	**7.81**
8	**5.77**	17.36	19.05	11.22	8.95
9	**6.16**	13.79	13.81	10.10	10.06
10	**7.09**	13.19	15.92	13.80	10.95
11	**7.97**	14.72	15.06	10.43	9.30
12	**6.98**	14.79	15.38	10.46	9.30
13	**7.19**	12.65	12.83	12.33	8.47
14	8.47	18.57	14.78	7.59	**7.03**
15	**6.58**	17.29	15.51	8.99	10.30
16	14.68	19.18	11.54	**9.47**	10.35
17	**6.43**	15.97	14.73	9.74	8.04
18	**6.50**	18.78	14.85	8.10	6.66
19	**7.18**	21.05	13.84	12.11	9.51
20	**6.51**	18.28	17.56	8.81	8.52
21	**5.87**	14.86	14.78	8.98	7.86
22	9.47	14.86	17.70	12.91	**7.72**
23	**7.23**	16.24	17.70	12.83	11.34
24	**6.48**	19.20	16.15	11.49	8.26
25	**8.44**	19.18	12.58	12.69	9.28
26	**8.18**	21.51	17.33	14.19	12.39
27	**7.65**	14.64	17.14	10.59	11.04
28	**8.72**	17.88	14.80	11.06	9.79
29	13.36	18.61	14.90	10.04	**9.62**
30	**6.79**	18.75	15.99	9.78	9.28
31	10.49	17.15	16.61	**8.79**	9.47
32	**6.10**	16.73	14.27	7.11	8.65
33	**7.80**	16.68	15.40	9.96	8.74
34	**8.78**	19.15	17.54	11.61	10.64
35	**7.89**	15.00	13.97	11.69	10.89
36	**6.64**	14.17	13.93	8.79	8.08
37	**8.04**	18.65	16.58	11.18	8.97
38	**7.27**	14.90	14.29	10.23	8.93
39	**6.19**	16.24	18.19	10.13	8.80
40	**7.45**	31.92	20.19	16.62	12.96
41	10.33	19.05	14.00	9.67	**7.09**
42	**10.57**	20.08	16.46	12.56	10.94
43	**6.49**	17.13	17.80	11.89	10.82

Table 3 (continued)

Test image	Proposed	Kuwahara-BM3D	Zayed-BM3D	TV-L1	WESNR
44	16.26	30.58	**12.34**	12.53	14.78
45	**7.51**	16.58	16.12	14.01	9.84
46	9.38	19.91	14.47	8.99	**8.80**
47	9.53	23.37	13.27	**7.70**	8.05
48	10.67	12.62	15.28	13.65	**10.43**
49	**10.33**	15.86	11.75	12.13	10.60
50	**11.13**	26.09	27.23	27.99	24.26
51	**7.97**	24.73	29.57	26.94	23.74
52	**7.82**	40.88	24.55	31.41	15.03
53	**7.09**	16.96	20.80	22.03	19.84
54	**5.77**	19.11	28.95	22.73	12.36
55	**9.35**	16.97	18.39	17.30	14.99

The results are obtained by the proposed, two-stage (2-stage) adaptive [38] and BM3D [16], presented in [44], Kuwahara-BM3D from [19], the total variation L1 [12, 35, 56], and WESNR from [29] methods. The noise assumed to be in 10% of the pixels affected by random valued impulsive noise

Bold values indicate the method with the best performance for the respective quality measure

method increased PSNR by up to 100% in some cases, when compared to the four competitive methods for the tested images. In some images, such as images 5,14,22,44,54, the PSNR is significantly higher in comparison with other methods. In terms of the SSIM, the proposed algorithm combining RANSAC and CS outperforms the competitive methods in many cases. It is interesting to note that, in most cases, the MS–SSIM index is above 0.97 for the proposed method. Additionally, comparing the values of the no-reference measure NIQE, we can see that the proposed method gives the most natural image in most of the cases.

From the given analysis, it is clear that the proposed RANSAC and CS based denoising method can outperform the other competitive approaches in most cases.

5 Conclusion

In this paper, we propose an image denoising approach based on RANSAC in conjunction with CS reconstruction. The CS reconstruction exploits the sparsity which each block of an image exhibit in the 2D-DCT domain. The RANSAC-based methodology combined with successive CS reconstructions is used to determine the set of pixels which can be considered as unaffected by the noise. Those pixels are used in the final CS reconstruction, to recover the remaining pixels, affected by the disturbance. Since the approach exploits signal sparsity, its efficiency is not affected by noise characteristics, such as distribution of the noise or its range of values. Moreover, even in cases when the noise corruption falls within the range of pixel values, the proposed approach is able to detect the impulsive noise. Numerical results on a relatively large set of images prove the efficiency of the proposed method. In particular, it outperforms several advanced state-of-the-art algorithms for image denoising. The quality is verified based on several objective metrics, and the results clearly support the presented theory. Our future work will be oriented towards main directions. In the first line of our future research, our goal is to develop a parallel, numerically highly efficient implementation of the proposed algorithm. The second line of our research will be oriented towards the development of an efficient combination of the presented RANSAC-CS denoising procedure and dictionary learning strategies, aiming to incorporate an alternative basis where image blocks exhibit improved sparsity. It is expected that such combination would lead to even further increased denoising capabilities of the presented approach.

Declarations The authors have no relevant financial or non-financial interests to disclose.

References

1. Aggarwal HK, Majumdar A (2016) Hyperspectral image denoising using spatio-spectral total variation. IEEE Geosci Remote Sens Lett 13(3):442–446
2. Arad B, Ben-Shahar O (2016) Sparse Recovery of hyperspectral signal from natural RGB images. In: Leibe B, Matas J, Sebe N, Welling M. (eds) Computer vision – ECCV 2016. ECCV 2016. Lecture notes in computer science, vol 9911. Springer, Cham, pp 19–35
3. Baraniuk RG (2007) Compressive sensing. IEEE Signal Proc Mag 24(4):118–121
4. Bartyzel K (2016) Adaptive Kuwahara filter. Signal Imag Video Process 10:663–670
5. Blumensath T (2011) Sampling and reconstructing signals from a union of linear subspaces. IEEE Trans Inf Theory 57(7):4660–4671
6. Boufounos P, Jacques L, Krahmer F, Saab R (2015) Quantization and compressive sensing. In: Boche H, Calderbank R, Kutyniok G, Vybíral J (eds) Compressed sensing and its applications. Applied and Numerical Harmonic Analysis, Birkhäuser, Cham, pp 193–237
7. Brajović M, Stanković I, Daković M, Stanković L (2020) The DCT domain sparsity-assisted detection and recovery of impulsively disturbed samples. Multimed Tools Appl:80. https://doi.org/10.1007/s11042-020-09998-w
8. Brajović M, Stanković I, Daković M, Ioana C, Stanković L Error in the Reconstruction of Nonsparse Images, Mathematical Problems in Engineering, 2018, Article ID 4314527, 10 pages, https://doi.org/10.1155/2018/4314527
9. Candès EJ, Romberg J, Tao T (2006) Robust uncertainty principles: exact signal reconstruction from highly incomplete frequency information. IEEE Trans Inf Theor 52(2):489–509
10. Candès EJ, Tao T (2005) Decoding by linear programming. IEEE Trans Inf Theory 52(12):4203–4215
11. Carrillo RE, Barner KE, Aysal TC (2010) Robust sampling and reconstruction methods for sparse signals in the presence of impulsive noise. IEEE J Select Topic Signal Process 4(2):392–408
12. Caselles V, Chambolle A, Novaga M. (2011) Total variation in imaging. Handbook Math Method Imag, Springer
13. Cetin AE, Tofighi M (2015) Projection-based Wavelet denoising. IEEE Signal Proc Mag 32(5):120–124
14. Chai X, Zheng X, Gan Z, Han D, Yiran C (2018) An image encryption algorithm based on chaotic system and compressive sensing. Signal Process 148:124–144
15. Chambolle A, Pock T (2011) A first-order primal-dual algorithm for convex problems with applications to imaging. J Math Imag Vis 40:120–145
16. Dabov K, Foi A, Katkovnik V, Egiazarian K (2007) Image denoising by sparse 3D transform-domain collaborative filtering. IEEE Trans Im Proc 16(8):2080–2095
17. Daubechies I, Defrise M, De Mol C (2004) An iterative thresholding algorithm for linear inverse problems with a sparsity constraint. Commun Pur Appl Math 57(11):1413–1457
18. Davis G, Mallat S, Avellaneda M (1997) Adaptive greedy approximations. Construct Approx 13(1):57–98
19. Djurović I (2017) Combination Of the adaptive Kuwahara and BM3d filters for filtering mixed Gaussian and impulsive noise. Sig Im and Video Proc 11:753–760
20. Djurović I (2017) QML-RANSAC: PPS and FM signals estimation in heavy noise environments. Signal Process 130:142–151
21. Djurović I (2018) QML-RANSAC If Estimator for overlapping multicomponent signals in the TF plane. IEEE Signal Process Lett 25(3):447–451
22. Donoho DL (2006) Compressed sensing. IEEE Trans Inf Theory 52(4):1289–1306
23. Donoho DL, Elad M, Temlyakov VN (2006) Stable recovery of sparse overcomplete representations in the presence of noise. IEEE Trans Inf Theory 52(1):6–18

24. Elad M (2010) Sparse and redundant representations: from theory to applications in signal and image processing. Springer, New York
25. Fadili MJ, Starck JL, Murtagh F (2009) Inpainting and zooming using sparse representations. Comput J 52(1):64–79
26. Figueiredo M, Bioucas-Dias J, Oliveira JP, Nowak RD (2006) On total-variation denoising: a new majorization-minimization algorithm and an experimental comparison with wavelet denoising. IEEE Int Conference Image Process (ICIP):2633–2636
27. Figueiredo MA, Nowak RD, Wright SJ (2007) Gradient projection for sparse reconstruction: Application to compressed sensing and other inverse problems. IEEE J Select Topic Signal Process 1(4):586–597
28. Image database (2021) Computer Vision group. University of Granada. http://decsai.ugr.es/cvg/CG/base.htm last opened
29. Jiang J, Zhang L, Yang J (2014) Mixed Noise removal by weighted encoding with sparse nonlocal regularization. IEEE Trans Image Process 23(6):2651–2662
30. Lebrun M (2012) An analysis and implementation of the BM3d image denoising method image processing on line
31. Liao X, Li K, Zhu X, Liu KJ (2020) Robust detection of image operator chain with two-stream convolutional neural network. IEEE J Select Topic Signal Process 14(5):955–968
32. Liao X, Yin J, Chen M, Qin Z (2020) Adaptive Payload distribution in multiple images steganography based on image texture features. IEEE transactions on dependable and secure computing (early access)
33. Liao X, Yu Y, Li Z, Qin Z (2020) A New payload partition strategy in color image steganography. IEEE Trans Circuits Syst Video Technol 30(3):685–696
34. Ma H, Nie Y Mixed Noise Removal Algorithm Combining Adaptive Directional Weighted Mean Filter and Improved Adaptive Anisotropic Diffusion Model, Mathematical Problems in Engineering, 2018, Article ID 6492696
35. Manolis L (2021) TV-L1 Image Denoising Algorithm (https://www.mathworks.com/matlabcentral/fileexchange/57604-tv-l1-image-denoising-algorithm), MATLAB Central File Exchange. Retrieved January 25, 2021
36. Mittal A, Soundararajan R, Bovik AC (2013) Making A “Completely blind” image quality analyzer. IEEE Signal Process Lett 20(3):209–212
37. Needell D, Tropp JA (2009) CosaMP: iterative signal recovery from incomplete and inaccurate samples. App Comp Harm An 26(3):301–321
38. Ramadan Z (2012) Efficient Restoration method for images corrupted with impulse noise. Circ Syst Signal Process 31(4):1397–1406
39. Rani M, Dhok SB, Deschmukh RB (2018) A Systematic review of compressive sensing: concepts. Implement Appl IEEE Access 6:4875–4894
40. Shah A, Bangash JI, Khan AW, Ahmed I, et. al (2020) Comparative Analysis of median filter and its variants for removal of impulse noise from gray scale images. Journal of King Saud University - Computer and Information Sciences
41. Stanković I, Brajović M, Daković M, Ioana C, Stanković L (2020) Quantization In compressive sensing: a signal processing approach. IEEE Access 8:50611–50625
42. Stanković I, Brajović M, Daković M, Ioana C, Stanković L (2020) Bit-depth quantization and reconstruction error in images. Sig Image Video Process 14(8):1545–1553
43. Stanković L, Brajović M, Stanković I, Lerga J, Daković M (2021) RANSAC-based signal denoising using compressive sensing. Circ Syst Signal Process 40. https://doi.org/10.1007/s00034-021-01654-4
44. Stanković I, Djurović I, Daković M (2018) Adaptive average BM3d filter for reconstruction of images with combined noise. 7th MECO 2018, Budva, Montenegro
45. Stanković I, Orović I, Daković M, Stanković S (2018) Denoising Of sparse images in impulsive disturbance environment. Multimed Tools Appl 77(5):5885–5905
46. Stanković S, Orović I, Sejdić E (2012) Multimedia signals and systems. Springer, New York
47. Stanković L, Sejdić E, Stanković S, Daković M, Orović I (2019) A tutorial on sparse signal reconstruction and its applications in signal processing. Circ Syst Signal Process 38:1206–1263
48. Stanković L, Stanković S, Amin MG (2014) Missing samples analysis insignals for applications to L-estimation and compressive sensing. Sig Proc 94:401–408
49. Stanković L, Stanković S, Orović I, Amin MG (2013) Robust time-frequency analysis based on the L-estimation and compressive sensing. IEEE Signal Process Lett 20(5):499–502
50. Studer C, Kuppinger P, Pope G, Bolcskei H (2012) Recovery of sparsely corrupted signals. IEEE Trans Inf Theory 58(5):3115–3130
51. Turlach BA (2005) On algorithms for solving least squares problems under an L1 penalty or an L1 constraint

52. Wang Z, Bovik AC, Sheikh HR, Simoncelli EP (2004) Image quality assessment: from error visibility to structural similarity. IEEE Trans Image Proc 13(4):600–612
53. Wang Z, Simoncelli EP, Bovik ACAC (2003) Multiscale structural similarity for image quality assessment. In: Proceedings of the 37th Asilomar Conference on Signals, Systems & Computers, 2003, 1398–1402. Pacific Grove, CA USA: IEEE, https://doi.org/10.1109/ACSSC.2003.1292216
54. Wright SJ (1990) Implementing proximal point methods for linear programming. J Optim Theory Appl 65(3):531–554
55. Yang Y, Sun J, Li H, Xu Z (2020) ADMM-CSNEt: a deep learning approach for image compressive sensing. IEEE Trans Pattern Anal Mach Intell 42(3):521–538
56. Zhang B, Zhu Z, Wang S (2016) A Simple primal-dual method for total variation image restoration. J Vis Commun Image Represent 38(C):814–823
57. Zhuang L, Ng MK (2020) Hyperspectral Mixed noise removal by L1-Norm-based subspace representation. IEEE J Selected Topic Appl Earth Observ Remote Sens 13:1143–1157